3-D Simulations of NSTAR Ion Thruster Plasma Environment

J. Wang*, J. Brophy†, and D. Brinza‡

Jet Propulsion Laboratory

California Institute of Technology, Pasadena

Abstract

Fully three-dimensional numerical models based on particle-in-cell with Monte Carlo collisions (PIC-MCC) simulations are developed to study ion thruster plasma interactions. 3-D simulation results for the NSTAR ion thruster plasma environment are presented. It is found that charge-exchange ion backflow will generate a plasma environment with a density of $10^6 cm^{-3}$ and a current density of $10^{-7} A/cm^2$ near the downstream-facing spacecraft surface. A particle simulation model is used to help the design and calibration of NSTAR diagnostic instruments.

1. Introduction

Electric propulsion devices are valued as a high-specific impulse class of space propulsion. To baseline the use of ion propulsion on spacecraft, NASA has initiated a technology demonstration and validation) program NSTAR (NASA Solar-Electric Propulsion Technology Application Readiness). Through ground tests and a space flight experiment, NSTAR will validate the life and performance of xenon ion thrusters, characterize the benefits and tradeoffs of xenon ion propulsion, and study the interactions and any potential impacts induced by ion thrusters.

It has long been recognized that the ion thruster plume could result in complex plasma interactions with the host spacecraft[1, 2, 13]. An ion thruster plume is composed of propellant efflux (high energy beam ions, neutralizing electrons, and unionized neutrals that escaped through the ion optics and from the neutralizer), nonpropellant efflux (material sputtered from thruster components and the neutralizer), and a low-energy charge-exchange plasma (generated through collisions between energetic ions and the neutrals within the plume). The plasma plume has raised various concerns. For instance, the charge-exchange ions can leave the primary plume and backflow toward the spacecraft. Backflow charge-exchange ions are thought to be the major mechanism for accelerator grid erosion. The deposition of the plume particles on thermal and optical surfaces may result in a change of the surface properties. Since charge exchange ions may interact with the solar arrays or any exposed conducting surface, the plume represents an additional charging mechanism. The plasma plume may also affect in situ measurements of ambient charged particles. Although the xenon ion engine has a substantially lower contamination potential compared to other types of propulsion devices, nevertheless, the interactions induced must be fully understood and their impacts quantified.

The purpose of this paper is to study ion thruster plasma interactions and quantify the ion thruster induced plasma environment for NSTAR.

Ion thruster plasma interactions have been studied for some time. Recently, Peng et al. used electrostatic PIC-MCC simulations to model the immediate downstream region of thruster accelerator grids and study grid erosion problems[7, 8, 9]. Samanta Roy et al. used electrostatic PIC simulations to model the far-downstream region and study charge exchange ion backflow[14, 4, 15]. Here, we present a detailed simulation of thruster induced plasma environment by considering a plasma plume emitted from a 3-dimensional, finite size, charged spacecraft.

2. Formulation and Approach

The NSTAR ion thruster and diagnostics will be flow II on the DS-1 spacecraft. Fig. 1 illustrates the IN- I space-

* Member Jet Propulsion Technical Staff, Advanced Propulsion Technology, Member AIAA

† Supervisor, Advanced Propulsion Technology, Member AIAA

‡ NSTAR Diagnostic Element Lead, Member AIAA

craft deployed configuration. Fig.2 shows a simplified DS 1 configuration that is used in our simulation. Considering the orientation of the Sun and the spacecraft orbit, we take the solar array surface facing the z direction, and the thrust direction in the x direction.

DS-1 is an interplanetary spacecraft. Since the interplanetray ambient plasma density is about $n_{ambient} \sim 1\ cm^{-3}$, the plasma environment surrounding DS-1 will be dominated by the ion thruster generated environment. Hence, we shall neglect the ambient plasma in our simulations.

NSTAR Parameters and Simple Calculations

The NSTAR ion thruster is a 30cm xenon ion thruster. Here we present some basic calculations relevant to the NSTAR ion thruster plasma environment.

Some of the basic parameters for the beam ions are: beam ion current: $I_b \simeq 1.76A$; exit beam velocity of the ions: $v_{bi0} \simeq 3.5 \times 10^6$ cm/s (Exit beam kinetic energy: $KE_{bi0} \simeq 1100eV$); temperature of the beam ions: $T_i \simeq 5001\{$ $(KE_{ti} \simeq 0.04eV)$; thermal velocity of the beam ions: $v_{ti} \simeq 1.6 \times 10^4$ cm/s.

From these parameters, the average beam ion current at thruster exit is

$$J_{bi0} = I/\pi r_T^2 \simeq 22.8\ A/m^2 \qquad (1)$$

and the average beam ion density at thruster exit

$$n_{b0} = J_{vi0}/ev_{bi} \simeq 4.3 \times 10^9\ cm^{-3} \qquad (2)$$

Measurements have shown that the beam ions form a diver-gcv]t flow with a divergence half angle about 15 to 20°. The radial beam current density profile is assumed to follow a Gaussian distribution:

$$|J_{bi}| \simeq J_{bimax} \exp(-(r/r_T)^2)\ r \leq r_T \qquad (3)$$

where J_{bimax} is the current density in the beam center. Although the actual distribution is more peaked[11].

The beam ions are neutralized outside the thruster exit by electrons emitted from the neutralizer. There have been no detailed measurements of the electron characteristics in the plume of the NSTAR thruster. For a simple analysis, one may assume that the electrons flow a Boltzman distribution

$$n_e \simeq n_{e,ref} \exp((\Phi - \Phi_{ref})/T_e) \qquad (4)$$

This assumption, which implies that the plume is quasi-neutral and the electron population is in equilibrium, has been used in almost all previous plume studies. The electron temperature T_e is typically thought to be $T_e \sim 1$ 5eV. Although some measurements suggest that T_e may be much lower than this value.

Assuming $T_e \sim 5eV$ (electron thermal velocity $v_{te} \simeq 9.4 \times 10^7$cm/s, and using other parameters presented above, one easily finds the following basic plasma parameters immediately outside the thruster exit:
plasma density: $n_0 \simeq 4.3 \times 10^9\ cm^{-3}$
electron and ion plasma frequencies: ω_{pe0} - 3.7 x 10^9rad/s and $\omega_{pi0} \simeq 7 \times 10^6$rad/s
Debye length: λ_{D0} -2.5 x 10^{-2}cm
ion accoustic velocity: $C_{s0} \sim \sqrt{T_e/m_i} \simeq 1.84 \times 10^5$cm/s

Expansion of Beam Ions

During normal ion thruster operation, electron emission keeps the exhaust plume quasi neutral and prevents the spacecraft from charging up significantly. Typically the spacecraft potential $\Phi_{s/c}$ is much lower than that of the beam ion kinetic energy, $|e\Phi_{s/c}| << KE_{bi0}$. The beam ions will mainly go along line of sight, $\vec{v}_{bi} \simeq \vec{v}_{bi0}$, and the core region of the ion beam will keep its coherent structure. Fig.3a shows the beam ion density n_b in the core region. Fig. 3b shows the beam ion density normalized by n_{b0} along the radial direction at thruster exit.

A high density plasma beam expanding into a vacuum or low density plasma region will also undergo an expansion when the beam density is mesothermal, $v_{ti} << v_{bi} << v_{te}$. Therefore, during normal thruster operations, an expansion fan similar to that of plasma expansion into a vacuum[16] is generated outside the beam region.

Assuming $T_e \simeq 5eV$, the Mach number for the beam ions al thruster exit is $M_{b0} = v_{bi0}/C_{s0} \simeq 18$. Let IIS denote θ an expansion angle starting from the beam direction, and $\theta_0 = \sin^{-1}(M_{b0}^{-1})$. Assuming the electrons follow the Boltzmann relation Eq(4) and following Wang and Hastings[16], one can snow that the beam ions will expand outward with a velocity

$$\vec{v}_\theta = C_s \qquad (5)$$

normal to their original line of sight direction. The beam ion density and the expansion angle θ have the following relationship

$$\ln\frac{n_i}{n_0} = \frac{e\Phi}{KT_e} = -\sqrt{M_0^2 - 1}(\theta_0 + \theta) - \frac{1}{2}(\theta_0 + \theta)^2 \qquad (6)$$

In Fig.4 we plot Eq(6) for three M_0, $M_0 = 2$,8,and 18. As Fig.4 shows, at $M_0 >> 1$, the ion density associated with the expansion fan is negligible for $\theta \geq 90°$. Hence, unless the spacecraft is very negatively charged or the beam is not quasi neutral, there is no interaction between the beam ions and the spacecraft.

Charge Exchange Ion Production

The unionized propellant forms a neutral plume. As Ref[4] snows, the density distribution of the neutral plume is modeled as that of a free molecular flow from a point source located at one thruster radius r_T behind the thruster exit. Hence, the density distribution of the neutral plume is given by:

$$n_n(R,\theta) = an_{n0}(1 - (1 + (\frac{r_T}{R})^2)^{-1/2})\cos\theta \quad (7)$$

where n_{n0} is the average neutral density at thruster exit, R is the distance to the point source, θ is the angle between R and the downstream axis, and a is a correction factor. n_{n0} is related to the ion beam via the following relationship[4]:

$$n_{n0} \simeq \frac{4n_{b0}v_{b0}}{C}(\frac{1}{\eta_p} - 1) \quad (8)$$

where $C = \sqrt{8kT_w/\pi m_{xenon}}$ is the mean thermal speed of the neutrals, and η_p is the propellant utilization efficiency. Typically, the thruster discharge chamber wall temperature is $T_w \simeq 500$K. For normal thruster operations, η_p range from 0.7 to 0.9. A significant higher neutral plume density may also be obtained either due to low propellant utilization or through extra neutral sources. Fig.5 snows the neutral plume density contours calculated from Eq(7)

Charge-exchange collisions will occur between the beam ions and the neutrals. Charge-exchange ions have been the primary concern for plume contamination. Next we do a simple calculation of the r-llarge-exchange collision freq uen cy $\nu_{cex} = n_n v_{bi}\sigma_{cex}(v_{bi}))$ and the charge-exchange ion production rate

$$dn_{cex}/dt = n_{bi}n_n v_{bi}\sigma_{cex}(v_{bi}) \quad (9)$$

near the thruster exit.

The charge-exchange collision cross section for xenon can be expressed by[12, 4]:

$$\sigma_{cex} = (k_1 \ln v_{bi} + k_2)^2 \times 1\ 0^{-20}\ m^2 \quad \textbf{(10)}$$

where v_{bi} is beam ion velocity with unit in m/s, $k_1 = -0.8821$, and $k_2 = 15.1262$. For $v_{bi} = 3.3 \times 10^4$ 111/s, $\sigma_{cex} \simeq 3.5 \times 10^{-15}\ cm^2$. Hence, at thruster exit, we find

$$\nu_{cex0} = n_{n0}v_{bi}\sigma_{cex}(v_{bi}) \simeq 6 \times 10^3 s^{-1}$$

and

$$dn_{cex0}/dt = n_{bi0}n_{n0}v_{bi}\sigma_{cex}(v_{bi}) \simeq 2.4 \times 10^{13} cm^{-3}s^{-1}$$

It is convenient to carry out the following normalization using plasma parameters near the thruster exit: $\hat{\nu}_{cex} = \nu_{cex}/\omega_{pi0}$, $\hat{n}_{cex} = n_{cex}/n_{bi0}$, $\hat{n}_{bi} = n_{bi}/n_{bi0}$, $\hat{n}_n = n_n/n_{n0}$, and $\hat{t} = t\omega_{pi0}$. The dimensionless charge-exchange collision frequency at thruster exit is $\hat{\nu}_{cex0} \simeq 8.24 \times 10^{-4}$ and the dimensionless charge-exchange production rate is

$$\frac{d\hat{n}_{cex}}{d\hat{t}} = \frac{\nu_{cex0}}{\omega_{pi0}}\frac{n_n}{n_{n0}}\frac{n_{bi}}{n_{bi0}} = 8.24 \times 10^{-4}\hat{n}_{bi}\hat{n}_{n0}$$

$d\hat{n}_{cex}/d\hat{t}$ is plotted in Fig.6.

Particle Simulation Model

In order to quantify the ion thruster plasma environment, a self-consistent calculation of the plasma particle orbits and the electrostatic potential is required. We have developed a set of fully 3-dimensional particle simulation programs consisting of hybrid electrostatic (ES), full particle ES PIC-MCC simulation, and full particle electromagnetic (EM) l'article-itl-(k]l Monte-Carlo collision (PIC-MCC) codes[21]. The simulation models and algorithms were discussed in Ref. [21].

Since our emphasis here is on the charge exchange ions and the plasma environment, we shall use the hybrid simulation code which only follows the ion trajectories and assumes that the electron density n_e is given by the Boltzmann distribution eq(4). This approach neglects the details near the thruster exit but l~rol'ides a more effective way to calculate ion dynamics in a global Scale.

Our simulation setup is shown in Fig.2. The spacecraft is modeled as a 3-dimensional box structure with a conducting surface and a surface potential Φ_w relative to the ambient. At each time step, the propellant ions are injected into the simulation domain from the thruster exit to form a beam described by eq(3). The neutral plume is treated as a steady state background described by eq(7). The charge-exchange ions are generated according to eq(9) based on the beam ion and neutral density profile. The trajectory of each charged particle is integrated from

$$\frac{dm\vec{V}}{dt} = \vec{F} = q(\vec{E} + \vec{V} \times \frac{\vec{B}}{c}), \quad \frac{d\vec{x}}{dt} = \vec{V} \quad (11)$$

using a standard leapfrog scheme, and the self-consistent electric field is obtained from the Poisson's equation

$$\nabla^2\Phi = -4\pi\rho \quad (12)$$

Since computationally it is not feasible to set the simulation domain large enough for the outer boundary to be the undisturbed ambient, a Neumann condition $\nabla\Phi_n = 0$ is used at all outer boundaries of the simulation domain.

3. Results and Discussions

Since the dimensions of the solar array for the DS 1 spacecraft has not yet been defined, here we shall consider the spacecraft configuration shown in Figure 2a (110 solar array). The spacecraft is taken to be a cubic box with dimension $1m$ x $1m$ x 1 m. In the simulation results presented here (with the exception of Figure 7), the spacecraft is located at $2 \leq x \leq 16$, $15 \leq y \leq 29$, and $15 \leq z \leq 29$. The thruster exit center is located at $x = 18$, $y = 22$, and $z = 22$. The thrust direction is in the x direction. The grid resolution is taken to be $d_{cell} \simeq 5.2$cm. In this paper, the number of grid points used for the simulation domain is 47 x 47 x 47 and the number of test particles is in the range of 10^6.

The parameters for the beam ions and charge-exchange ion production have been discussed in the last section. The spacecraft potential needs to be determined based on the global spacecraft charging condition. Under normal thruster operations, the spacecraft can be charged only to a low potential. Here, we take the spacecraft potential to be $-\Phi_{s/c}/T_e \simeq 3$ ($KE_{bi0}/|e\Phi_{s/c}| \simeq 33.3$).

In Fig. 7 though Fig. 11, we show simulation results on a xy plane cutting through the spacecraft and thruster center at $z = z_{thruster} = 22$ (the "center xy plane"). Fig.7 shows the potential contours for the no beam situation. When the thruster is operating, since $KE_{bi0}/|e\Phi_{s/c}| >> 1$ and the beam is quasi neutral, the beam ions are not influenced by the potential field. The beam ion positions are shown in Fig.9a. As Fig.8 shows, the structure of the potential field is dominated by the disturbance from the high density ion beam. Since the electrons are much more mobile than ions, the beam center has a higher potential.

Collisions between the beam ions and the neutral background generate charge exchange ions. The charge exchange ion production rate is proportional to the neutral density and beam ion density, as shown in Figure 6. In contrast to the beam ions, the motion of the charge exchange ions are influenced by the potential field due to their low kinetic energy. Fig. 9b and 9c are a x-y position plot and a v_x/C_s-x phase space plot for the charge-exchange ions respectively.

Fig. 10 shows the normalized total ion density, $\hat{n}_{ion} = n_{ion}/n_{bi0}$, and the charge exchange ion density, $\hat{n}_{cex} = n_{cex}/n_{bi0}$, on the center xy plane. Fig.11a shows the normalized charge-exchange ion current density $\hat{J}_{cex}$. Fig.11b shows the directions of the charge-exchange ion current $\vec{J}_{cex}/|J_{cex}|$. It is obvious that the potential field influences the charge exchange ions in two ways, First, due to the negative potential on the acceleration grid, charge exchange ions produced near the thruster exit will be accelerated towards the thruster exit. This back-flow causes erosion on the acceleration grids. Second, since the plume center has a higher potential, charge exchange ions produced within the beam can flow radially outward the beam region. It is well recognized that, once outside the plume, charge exchange ions may become a potential contamination source.

once outside the beam, charge-exchange ions fall into the influence of the global potential field surrounding the spacecraft. For an interplanetary spacecraft, since the ambient plasma density is low, there will always be a thick sheath surrounding the spacecraft. Except for those charge-exchange ions generated right downstream of the thruster, the collection of charge-exchange ions by the spacecraft is similar to the current collection by a probe in the orbital motion limited regime. As Fig.10 Snows, the outflow of charge exchange ions form a wing shaped strucutre.

In Fig.12 and 13, we snow charge exchange ion number density and current density at several downstream distances on on the center xy plane ($z = 22$). Fig. 12 shows $\hat{n}_{ion}$ and $\hat{n}_{cex}$ at three downstream distances: $x = 19$ (immediately downstream of the thruster); $x = 29$ (55cm downstream of the thruster); and $x = 38$ (101cm downstream of the thruster). In Fig. 13 we compare Jeer at thruster exit, $x = 18$, and at spacecraft surface $x = 16$. We find the charge exchange ion desnity $n_{cex}/n_{bi0} \sim 0.33$, or $n_{cex} \sim 1.4 \times 10^9 cm^{-3}$ near thruster exit. The spacecraft's downstream surface sees a charge ion density $n_{cex}/n_{bi0} \sim 0.001$, or $n_{cex} \sim 4 \times 10^6 cm^{-3}$ (when $z = 22$). Note this density is significantly larger than the interplanetary ambient plasma denity.

In Fig. 14 and Fig. 15, we show simulation results on a xy plane cutting through different z locations: $z = 24$ (immediately outside of the thruster); $z = 25$ (5.2cm outside from the thruster); and $z = 28$ (5.2cm inside from the spacecraft edge). Not surprisingly, the charge ion density decreases as one moves further away from the thruster center.

As evident from the vector plot of $\vec{E}$ and the results shown from Fig. 10 through 15, we find that a symmetrically shaped spacecraft charged to a few T_e can not pull a significant amount of charge-exchange ions to the upstream surface of the spacecraft. Therefore, the ram side environment is not disturbed by the thruster operation. However, this conclusion may not hold if the spacecraft is highly differentially charged.

4. Summary and Conclusions

We have developed a set of fully three-dimensional numerical models based on parti cle-in- cell with Monte Carlo collisions (PIC-MCC) simulations to study ion thruster plasma interactions. In this paper, we applied a hybrid PIC-MCC model to obtain the thruster induced environment for NSTA R. Our simulations show that the charge-exchange ion density is about $n_{cex}/n_{bi0} \sim 10^{-3}$ ($n_{cex} \sim 4 \times 10^{6} cm^{-3}$ near the downstream - facing sp acecraft surface and about $n_{cex}/n_{bi0} \sim 0.3$ ($n_{cex} \sim 1.4 \times 10^{9} cm^{-3}$ at thruster exit. The charge-exchange ion backflow current density is about $J_{cex} \sim 1 \times 10^{-7} A/cm^2$ near the downstream facing spacecraft surface and about $J_{cex} \sim 5 \times 10^{-6} A/cm^2$ at thruster exit. Therefore, under normal thruster operating conditions, charge-exchange ions should not alter a spacecraft's charging environment. The uncertainties in results presented in this paper come from the assumption of electron Boltzmann distribution and the assumed value of electron temperature. Our recent full particle simulations suggested that the electron distribution sensitively depends on the interations between beam ions and electrons[22]. The electron characteristics are being studied in detail in our ongoing research.

This modeling study is performed to compliment the NSTAR diagnostics. Our particle simulation model is currently used to help the design and calibration of NSTAR diagnostic instruments. In the future, our numerical results will also be compared with experimental data obtained from ongoing ground tests of the NSTAR thruster as well as in situ measurements abord the D S-1 spacecraft.

Acknowledgement

This work was carried out by the Jet Propulsion Laboratory, California Institute of Technology under a contract with NASA. Access to the Cray supercomputers was provided by funding from NASA Offices of Mission to Planet Earth, Aeronautics, and Space Science.

References

[1] M.R. Carruth Ed, Experimental and analytical evaluation of ion thruster/spacecraft interactions. JPL Publication 80-92, 1981.

[2] M.R. Carruth, A review of studies on ion thruster beam and charge-exchange plasmas *AIAA 82-1994*, 1982.

[3] W.D. Deininger Electric propulsion produced environments and possible interactions with the SP-100 power system. *AIAA 85-2046*, 1985.

[4] N. Gatsonis, R. Samanta Roy, and J. Hastings, Numerical investigation of ion thruster plume backflow, *AIAA 94-3140*, 1994.

[5] S. Karmesin, P. Liewer, and J. Wang, 3-D electromagnetic parallel PIC in nonorthogonal meshes, IEEE ICOPS'95, 1995.

[6] J. Monheiser and J. Wilbur, An experimental study of impingement ion production mechanisms, *AIAA 92-3826*, 1992.

[7] X. Peng, W. Ruyth, and D. Keefer, 3D particle simulation of grid erosion in ion thrusters, *AIAA 91-119*, 1991

[8] X. Peng, W. Ruyth, and D. Keefer, Comparison of 2D and 3D models of grid erosion in an ion thruster, *AIAA 91-2120*, 1991.

[9] X. Peng, W. Ruyth, and D. Keefer, Further study of effect of the downstream plasma condition on accelerator grid erosion in an ion thruster, *AIAA 92-?829*, 1992.

[10] J. Pelk, J. Brophy, and J. Wang, Spatial and temporal variation of sputter erosion on the accelerator electrode of a 2-Grid, 30-cm ion optics *AIAA 95-2924*, 31st Joint Propulsion Conference, 1995.

[11] J. Polk and J. Brophy, 32nd Joint Propulsion Conference, 1996.

[12] D. Rapp and W.E. Francis, Charge exchange between gaseous ions and atoms, *J. Chemical Physics*, 37(1 1), 1962, pp2631.

[13] R.S. Robinson, H.R Kaufman, and D.R. Winder Simulation of charge exchange plasma propagation near an ion thruster propelled spacecraft *AIAA 81-0774*, 1981.

[14] R. Samanta Roy, D. hastings, and N. Gatsonis, Modeling of ion thruster plume contamination, *AIAA 95-3138*, 1994.

[15] R. Samanta Roy, Numerical simulation of ion thruster plume backflow for spacecraft contamination assessment, Ph D. thesis, MIT, 1995.

[16] J. Wang and D. Hastings, Ionospheric plasma flow over large high-voltage space platforms. II: The formation and structure of plasma wake, *Physics of Fluids B*, 4(6), 1992, pp1615-1629.

[17] J. Wang, P. Liewer, and V. Decyk, 3D electromagnetic plasma particle simulations on a MIMD parallel computer, *Computer Physics Comms.*, 87, 1995, pp35-53.

[18] J:. Wang, R. Biasca, and 1'. Liewer, , 3D electro magnetic Monte Carlo]Jarticle-irl-cell simulations of critical ionization velocity experiments in space *J. Geophys Res.*, 101(A1), 1996, pp371- 382.

[19] J. Wang, 1'. Liewer, and E. Huang, 3D electro magnetic Monte Carlo particle-in-cell simulations on MIMD parallel computer, *AIAA 95-059 .?,1995.*

[20] J. Wang, J. Brophy, 1'. Liewer, and G. Murphy, Modeling ion thruster plumes, *AIAA 95-0596,1995.*

[21] J. Wang and J. Brophy, 3-D Monte-Carlo particle-ill-cell simulations of ion thruster plasma interactions, *AIAA 95-2826,1995.*

[22] J. Wang and S. Lai, Virtual anodes in ion beam emissions in space: Numerical simulations, *AIAA 96-2299*,1996.

Figure Captions

Figure 1: 1) S- 1 and NSTAR configuration.

Figure 2: Model setup. a) Spacecraft. b) Spacecraft with deployed solar arrays.

Figure 3: The core region of the ion beam (when the ion beam is neutralized). Upper pannel: beam ion density contours (cont our level: n_{bi}/n_{bimax} = 0.1, 0.2,..,1.). Lower pannel: $\hat{n}_{bi} = n_{bi}/n_{bi0}$ along the radial direction at thruster exit.

Figure 4: Quasineutral expansion of a plasma beam, O vs. $\hat{n}_{beam}$. M_{b0} = 18 (solid line), M_{b0} = 8 (dashed line), and M_{b0} = 2 (dotted line).

Figure 5: Neutral background density contours on the center xy plane.

Figure 6: Charge-exchange ion production rate. Contours for $d\hat{n}_{cex}\,c\hat{t}$ on the center xy plane. (Contour level: ((lil$_{cex}$/fit)/?il/$_{cex}$O = 0.01. **0.05, 0.1, 0.5, 1.,** 1.5).

Figure 7: Potential contours on the center xy plane for no beam situation

Figure 8: Potential contours (a) and $\vec{E}$ field (b) on the center xy plane. Simulation case A.

Figure 9: Beam ion positions (a), charge- exchange ion positions (b), and v_x/C_s vs. x phase plot for the charge-exchange ions within the center layer.

Figure 10: a) Total ion density contours (contour level: n_{ion}/n_{bi0} = 10^{-4}, 5×10^{-4}, 10^{-3}, 5×10^{-3}, 10^{-2}, 5 x 10-9, 0.1, 0..5, 1., 1 .5). b) Charge-exchange ion density contours (contour level: n_{cex}/n_{bi0} = 10- 4,2X10-4, 4X IO"4,6X IO-4, 8X IO-4, 1O-3, 2X IO"3,4X1 O-3, 6 x 10^{-3}, 8×10^{-3}, 10^{-2}, 2×10^{-2}, 4×10^{-2}, 6x 10^{-2}, $8\times$ **10-^{2}**, **0.1,0.2,(}.3)

Figure 11: Charge-exchange ion current Vector plots for $\vec{J}_{cex}$ (a) and $\vec{J}_{cex}/|J_{cex}|$ (b).

Figure 12: Charge exchange ion number density at several downstream distances on the center xy plane (z= 22): immediately downstream of thruster (a), 55cm downstream (b), 101cm downstream.

Figure 13: Charge exchange ion current density J_{cex} at thruster exit (x = 18, solid line) and at spacecraft surface (x = 16, dotted line).

Figure 14: Potential contours on a xy plane cutting through different z locations: z = 24 (a), z = 25 (b), and z = 28 (c).

Figure 15: Charge exchange ion density contours on a xy plane cutting through different z locations: z = 2 4 (a), z = 25 (b), and z = 28 (c).

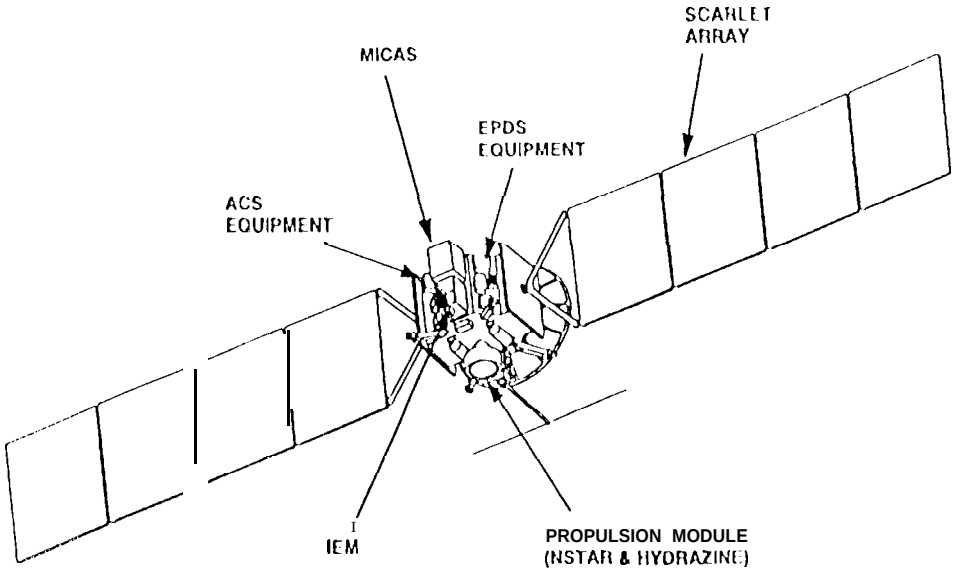

Figure 1

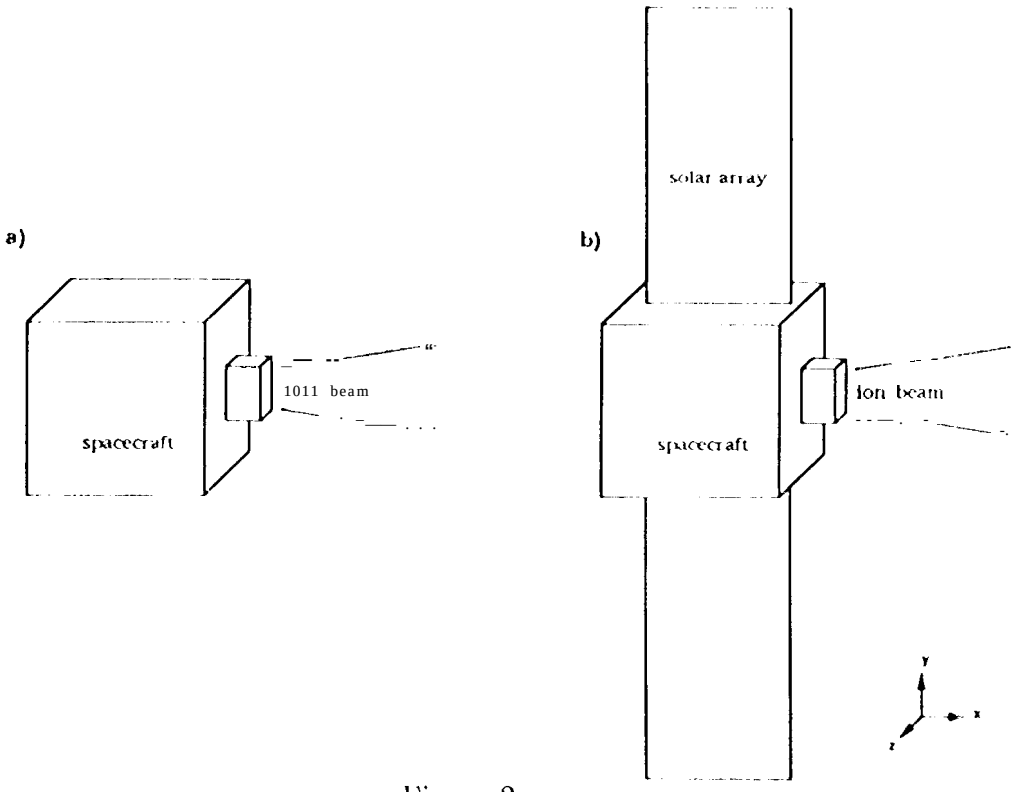

Figure 2

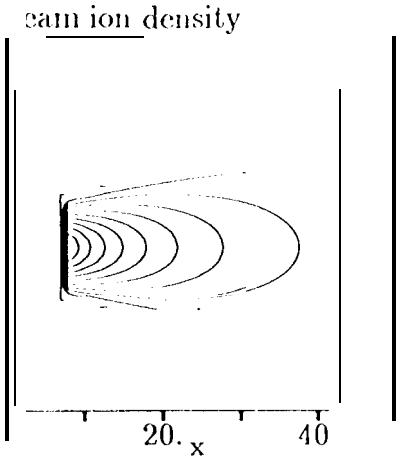

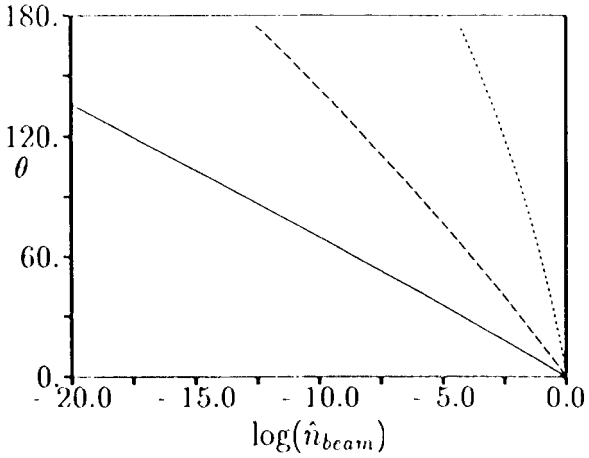

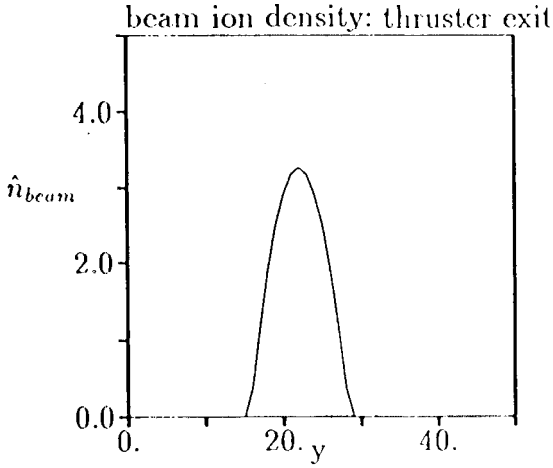

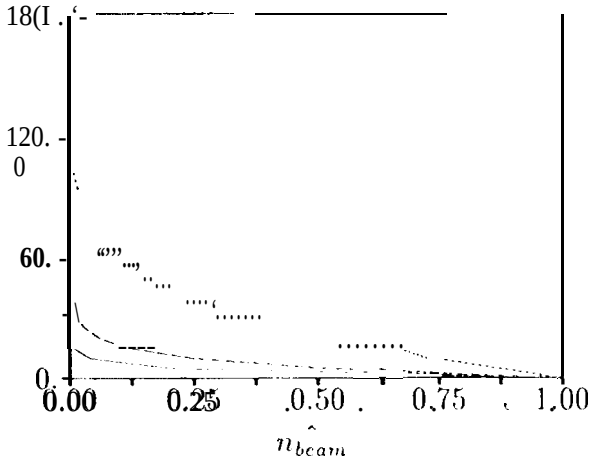

Figure 3

Figure 4

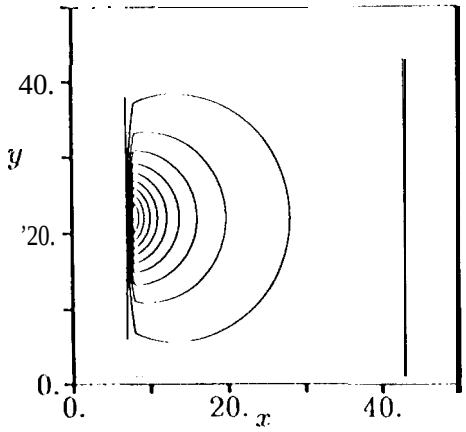

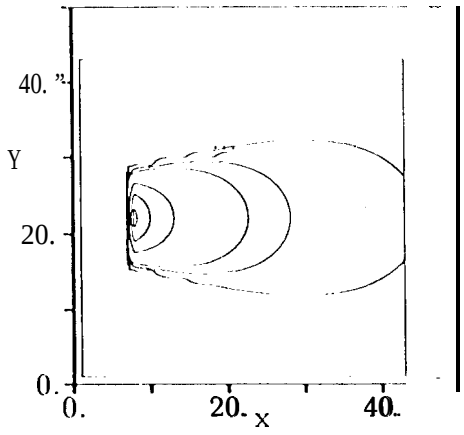

Figure 5

Figure 6

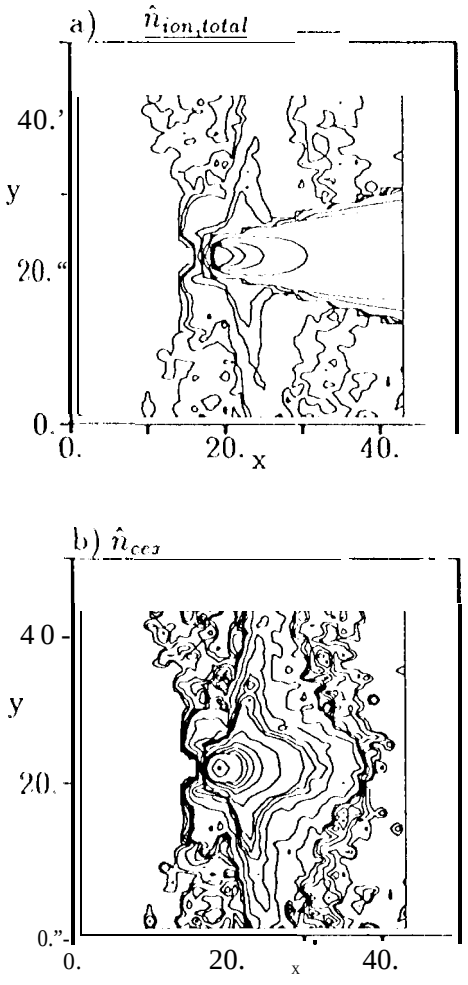

Figure 10

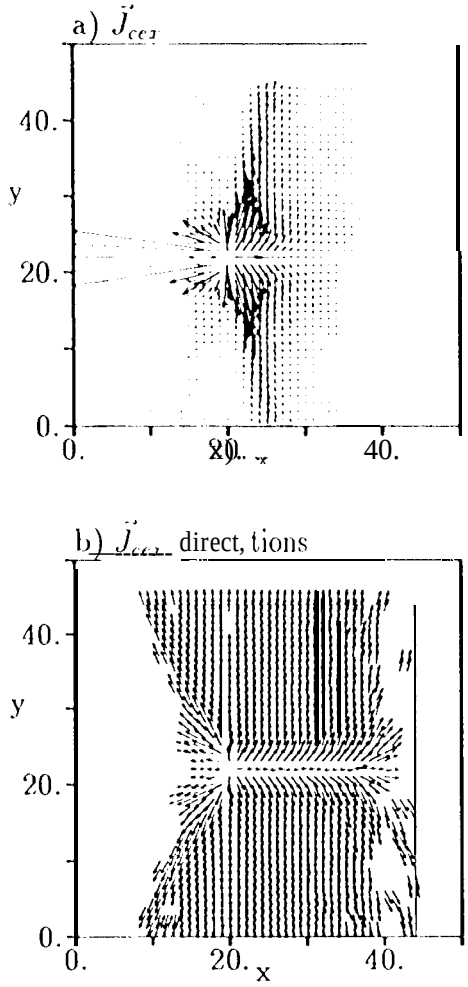

Figure 11

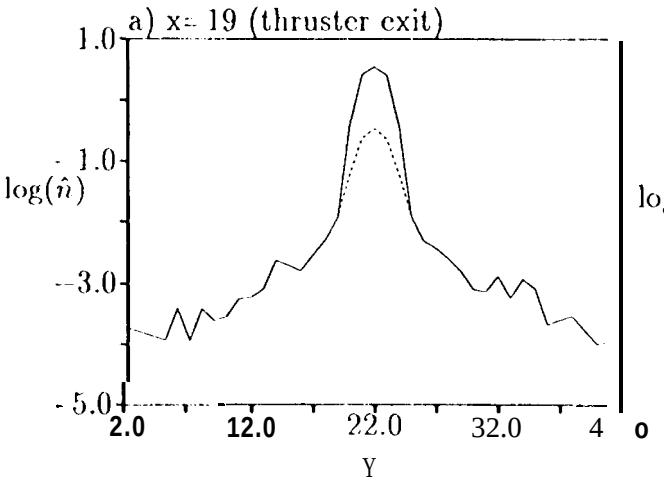

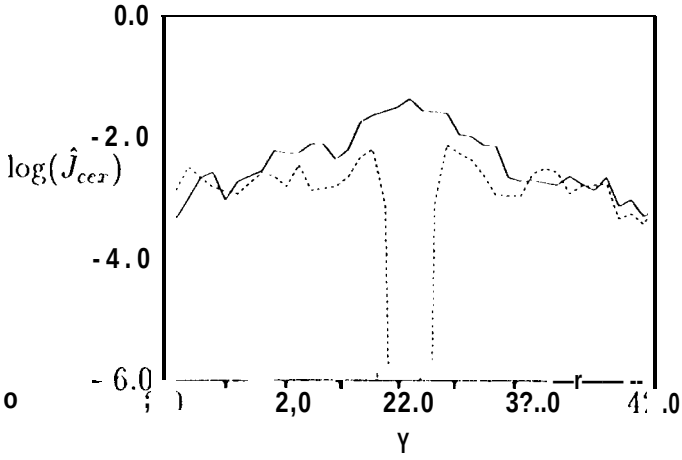

Figure 13

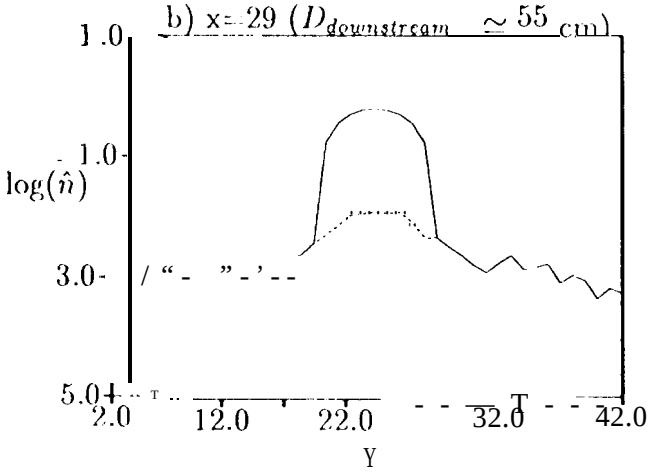

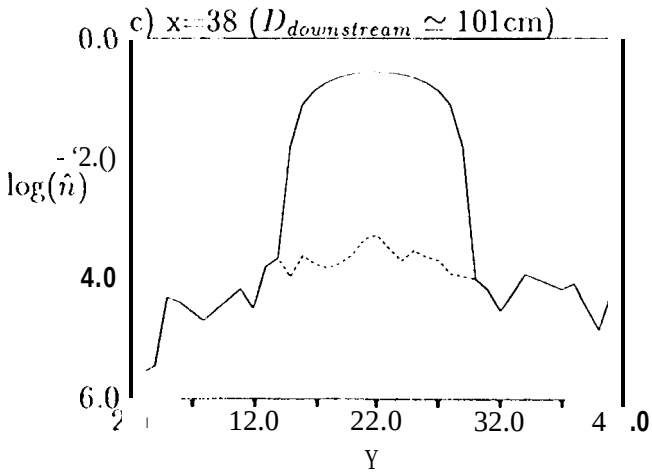

Figure 12

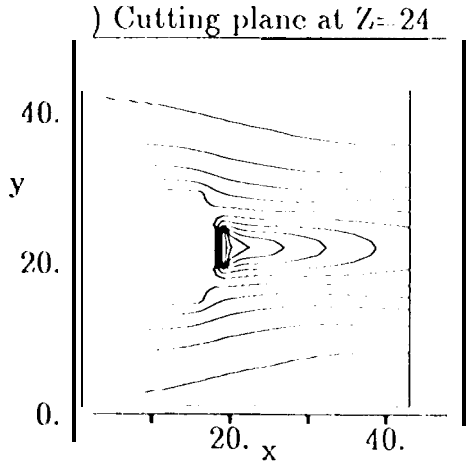

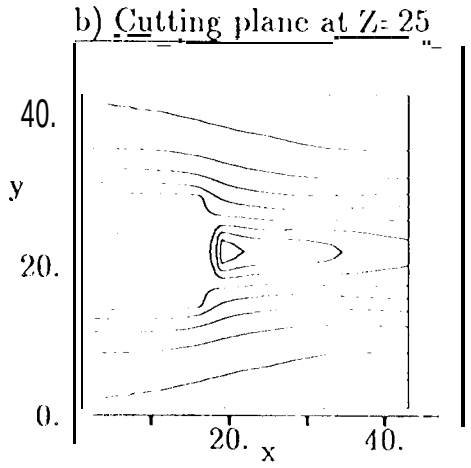

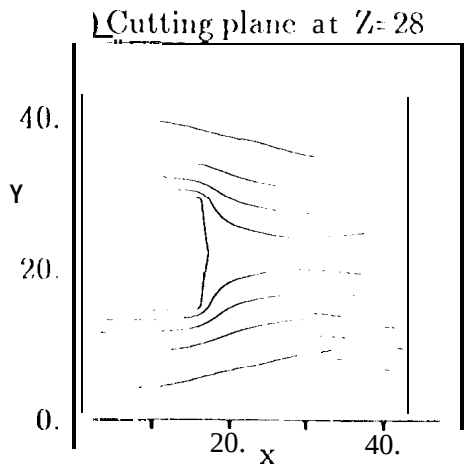

Figure 14

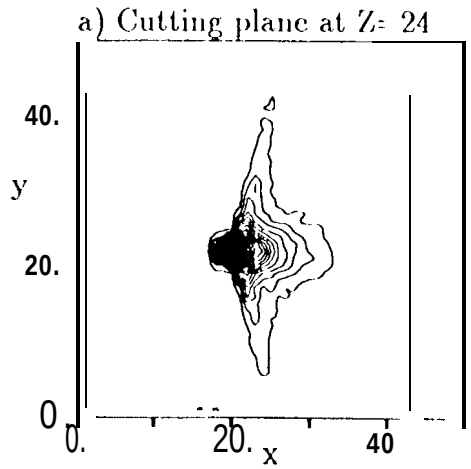

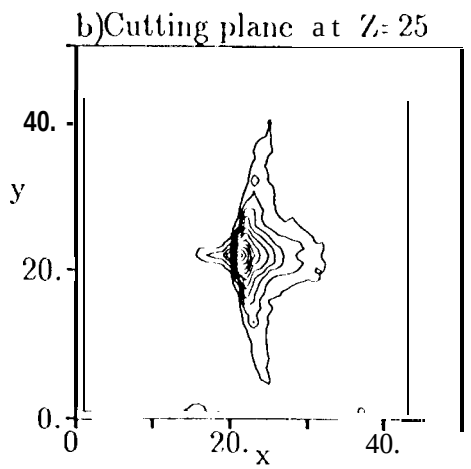

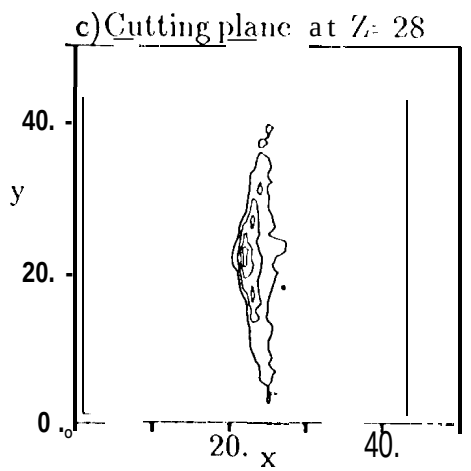

Figure 15